

Communication

Simulation Design for Rutile-TiO₂ Nanostructures with a Large Complete-Photonic Bandgap in Electrolytes

Sachiko Matsushita *, Mikiro Hayashi, Toshihiro Isobe and Akira Nakajima

Department of Metallurgy & Ceramics Science, Graduate School of Science & Technology, Tokyo Institute of Technology 2-12-1-S7-8, Ookayama, Meguro-ku, Tokyo 152-8552, Japan; E-Mails: hayashi0331@gmail.com (M.H.); isobe.t.ad@m.titech.ac.jp (T.I.); nakajima.a.aa@m.titech.ac.jp (A.N.)

* Author to whom correspondence should be addressed; E-Mail: matsushita.s.ab@m.titech.ac.jp; Tel.: +81-3-5734-2525; Fax: +81-3-5734-3355.

Received: 4 April 2012; in revised form: 9 October 2012 / Accepted: 10 October 2012 /

Published: 26 October 2012

Abstract: The photonic bands of various TiO₂ 2D photonic crystals, *i.e.*, cylindrical, square and hexagonal columns connected with/without walls and filled with acetonitrile, were investigated from the perspective of dye-sensitized solar cells. The finite-difference time-domain methods revealed that two-dimensional (2D) photonic crystals with rods connected with walls composed of TiO₂ and electrolytes had complete photonic band gaps under specific conditions. This optimally designed bandgap reaches a large $\Delta\omega/\omega_{\text{mid}}$ value, 1.9%, in a triangular array of square rods connected with walls, which is the largest complete 2D bandgap thus far reported for a photochemical system. These discoveries would promote the photochemical applications of photonic crystals.

Keywords: photonic band diagram; photonic band gap; photocatalyst; dye-sensitized solar cell; electrochemical reaction

1. Introduction

The concept of coupling a conventional dye-sensitized nanocrystalline TiO₂ film with a photonic crystal has been actively pursued [1–10]. A promising idea is to enhance the relaxation-light harvesting by multiple scattering to improve the efficiency of dye-sensitized solar cells. We pursued coupling the conventional dye-sensitized nanocrystalline titanium oxide (TiO₂) film with a photonic crystal, which

inhibits spontaneous emission [11] and light propagation [12], in order to enhance the spectral response to the red end of the dye absorption band [13]. The short-circuit photocurrent efficiency across the visible spectrum (400–750 nm) of the electrode comprising a bilayer of inverse opal photonic crystal—nanocrystalline dye-sensitized titanium dioxide could be increased by about 26%, relative to an ordinary dye-sensitized nanocrystalline TiO₂ photoelectrode [7,14].

Among this research, the authors have paid attention to the dye emission in the solar cell. The key component of the dye-sensitized solar cell is the photoelectrode, which consists of a dye molecule, titanium oxide (TiO₂), and a transparent electrode. The incident light at the photon energy of $h\nu_1$ excites the dye molecule. The excited electron relaxes to a lower excited state in the dye and then a certain fraction of it is injected into the conduction band of TiO₂, resulting in the extraction of photocurrent from the electrode. Another fraction directly relaxes to the ground state with an emission of photon energy of $h\nu_2$, resulting in the reduction of photon-to-electron conversion efficiency. We would like to introduce a photonic crystal structure to inhibit the emission from the dye at $h\nu_2$ for enhancement of electron injection efficiency. This idea allows us to be free from the consideration of the illumination direction, because the illumination wavelength $h\nu_1$ differs from the emission wavelength $h\nu_2$. Our idea had been partially proved using inverse-opal-type photonic crystals; however, since inverse-opals were not shown the full-photonic band gaps, this former result is fraught with uncertainty. To prove our idea, we need the full photonic band gap structure composed of TiO₂ and electrolyte.

This light emission from the dye is not a major problem in the Ruthenium dye, which is the most efficient dye in the DSCs. However, Ruthenium is a rare-metal resulting in the high-cost preparation of the DSCs. If we would like to use non-rare metal dyes, the light emission from the dyes becomes the one of the major problems because of the low electron injection efficiencies to the TiO₂ [15]. Using this concept, the authors tried to inhibit the spontaneous emission from the Chlorine-e6 dye in a dye-sensitized photoelectrode by the photonic crystal structures, resulting in an increase in photon-to-electron conversion efficiency per mol of dye [8]. The improvement of monochromatic incident photon-to-current conversion efficiency (IPCE) in the dye-sensitized solar cells using quasi-photonic crystals was convinced in the author's previous paper and patent [8,16]. However, TiO₂ inverse opal structures only exhibit a pseudogap not a complete photonic bandgap. To inhibit the spontaneous emission, the complete photonic bandgap, or complete photonic bandgap in a 2D structure at least, is necessary. Not only for such dye-sensitized solar cells, an air-guiding photonic bandgap fiber was also examined as a highly sensitive gas sensor [17], and a liquid-filled hollow-core photonic crystal fiber was studied as a highly controlled photochemical reactor [18]. The current problem of this field is the lack of the complete-photonic bandgap structures composed of the materials of the photochemical systems.

However, few reports are available on complete-photonic-bandgap (CPBG) structures composed of photochemically functional materials such as photocatalysts. Recently, the authors computationally discovered both two-dimensional (2D) and three-dimensional (3D) CPBG structures composed of TiO₂ in electrolytes by plane-wave expansion method [2]. The discovered 3D structures were the diamond-log structures composed of TiO₂ rods in electrolytes and the inverse diamond-log structures composed of electrolyte rods in a TiO₂ slab. However, as regards dye-sensitized solar cells when using popular dyes in ruthenium complexes, for example, the single cell size of a rutile-TiO₂ photonic crystal

with the CPBG centered near the dye emission wavelength ($\lambda \sim 600$ nm) must be 307 nm, which corresponds to a 70-nm rod diameter. Such a feature size is beyond the fabrication capabilities of the current 3D lithography methods [19].

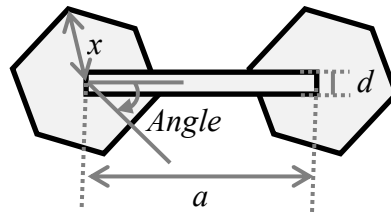
The 2D CPBG structures detailed in the author's previous report [2] were triangular lattices of electrolytes composed of square rods drilled into a TiO₂ slab. To fabricate such a structure with the bandgap centered at the emission maximum of ruthenium complex, the width of the square holes and TiO₂ canals should be 396 and 164 nm, respectively. Such 2D structures can be produced by electron-beam lithography. However, the gap-midgap ratio $\Delta\omega/\omega_{\text{mid}}$ of the CPBG was only 1.2%. In this study, the authors attempted to determine the photochemically functional 2D periodic structures exhibiting wider CPBG while considering the following recent discoveries by other researchers: bandgaps for transverse-electric (TE) polarization are favored in a lattice of an isolated high- ϵ region, bandgaps for transverse-magnetic (TM) polarization are favored in a connected lattice, and two geometric parameters are required to balance the band edges of TE and TM polarizations to obtain the optimal complete bandgap [20].

2. Calculation

2.1. Structural Design

The optical properties of photonic crystals are governed by the geometry and difference in index contrasts. In general, a large difference in index contrasts is required for CPBG [21]. To increase the difference in the index contrasts of semiconductors and electrolytes, which comprise a photochemical system, we exclusively studied rutile-TiO₂ structures ($n = 2.9$ and 2.6 for $C_{//}$ and C_{\perp} , respectively, at $0.6 \mu\text{m}$ light wavelength by SOPRA N & K database) with an index contrast of 1.55 in acetonitrile ($n = 1.35$), rather than anatase-TiO₂ structures ($n = 2.55$). Here we should mention that TiO₂ refractive indexes (both rutile and anatase) exhibit a strong dispersive behavior in the UV and in the visible. This feature can be problematic to fabricate the structure, but it can also be an opportunity, because the growth of n with the frequency leads to the possibility of multiple CPBGs, or to their widening. In this research, tentatively, we fixed the refractive index at 2.9. We should also point out that, talking from the viewpoint of the photon-to-electron conversion efficiency, anatase-type TiO₂ has been a promising material for dye-sensitized solar cells, at one sun light intensity, because of its surface chemistry and potentially higher conduction-band edge energy, even though rutile is potentially cheaper to be produced and has superior light scattering characteristics.

Complete-photonic-bandgap structures of 2D lattices composed of square air rods drilled into silicon [22] and the influence of rotating non-cylindrical air rods in a dielectric background [23] have been reported. Considering these studies, we investigated the tetragonal or triangular arrays of TiO₂ composed of cylindrical, square, and hexagonal rods in electrolytes and electrolytes composed of cylindrical, square, and hexagonal rods in TiO₂. Each rod was connected to its nearest neighbors by thin walls. The simulation parameters included the width of the wall, d ; the radius/length of each side, x ; and the rotation angle of the rod, $Angle$. The simulation range and resolution of each parameter are summarized in Table 1. All possible values of d , x , and $Angle$ in the structure were examined. Here we set the distance between the centers of the columns, a , as 1.

Table 1. Simulation range of each parameter.

	Resolution	Cylindrical	Square	Hexagonal
d	1×10^{-5}	0.00–0.50	0.00–0.50	0.00–0.50
x	1×10^{-4}	0.01–0.50	0.01–0.50	0.01–0.50
Angle [°]	0.01	-	(-45)–(+45)	(-60)–(+60)

2.2. Simulation Methods

Photonic bands were determined using photonic band calculation software (*BandSOLVE*, Rsoft Design Group), which is based on the plane-wave-expansion method. A Windows computer (Dell precision T1500, Intel (R) Core (TM) i7 CPU, 860@2.80 GHz) was used for the calculations. The number of calculated bands was 16. Path Division number was examined from 8 to 256.

3. Results and Discussion

3.1. Photonic Band Diagram of Each Structure

After precise calculations to check the dependence of the band diagram stability on the path division number, we select 128 as the path division number. As previously mentioned, bandgaps for TE polarization are favored in a lattice of isolated high- ϵ region and those for TM polarization are favored in a connected lattice. This connected structure was precisely studied by Chern *et al.* [20,24] On the basis of their reports, we examined arrayed electrolytes and TiO₂ rods connected by walls composed of the same material as that of the rods.

The tetragonal arrays of both electrolytes and TiO₂ rods exhibited either TE or TM bandgaps but no CPBG, regardless of the presence of wall-connected rods. On the contrary, triangular arrays of TiO₂ composed of cylindrical, square, and hexagonal columns with the walls exhibited CPBG in electrolytes; however, structures without the walls exhibited no CPBG in our calculations. The walls, introduced to make the TE fields follow the high- ϵ paths from site to site, appeared insufficient to localize the TE band. Instead, the narrow spaces between the columns in the triangular arrays acted as the high- ϵ paths.

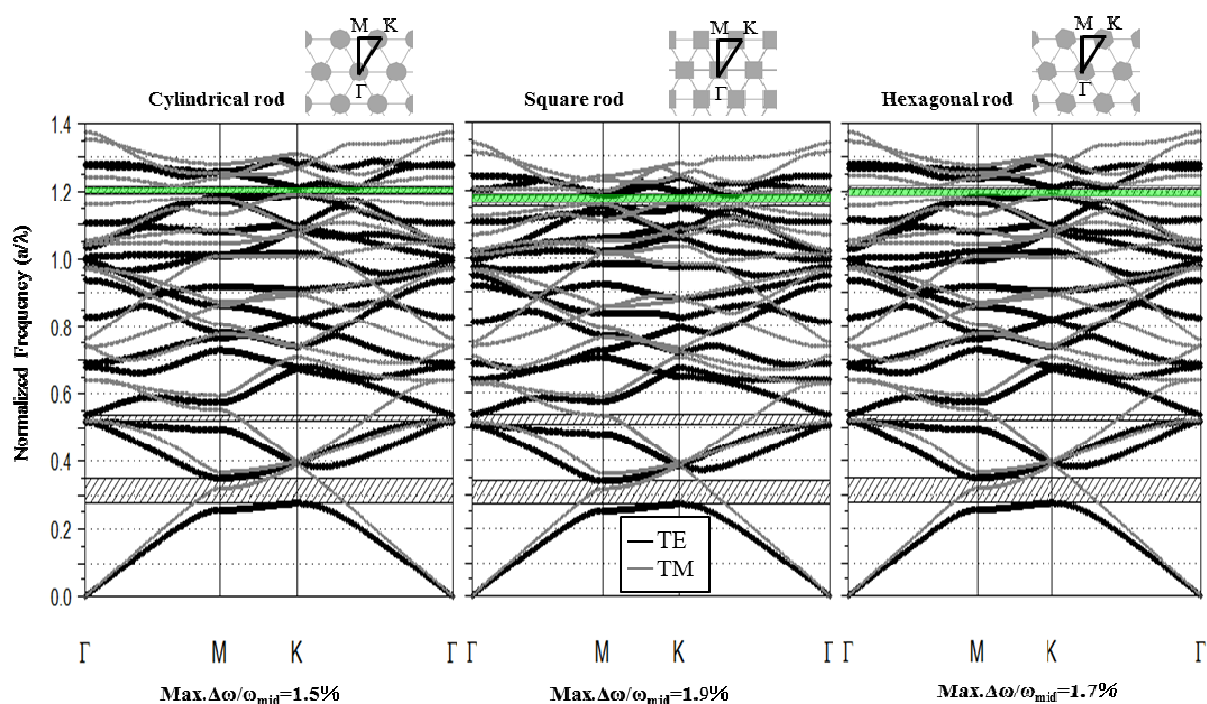
The photonic band diagrams with the maximum $\Delta\omega/\omega_{\text{mid}}$ value in the triangular arrays of cylindrical, square and hexagonal columns are depicted in Figure 1. The CPBGs, represented as mesh areas, are located around $a/\lambda = 1.2$ in each band diagram. The maximum $\Delta\omega/\omega_{\text{mid}}$ value in cylindrical, square, and hexagonal columns with the walls were 1.5%, 1.9%, and 1.7%, respectively, which were larger than the 1.2% previously reported. The maximum gap–midgap ratio for cylindrical columns corresponded to $x/a = 0.26$; for square columns, to $x/a = 0.24$ and $\text{Angle} = -0.3^\circ$; and for hexagonal columns, to $x/a = 0.2875$ and $\text{Angle} = 43^\circ$ and -16.5° . The maximum complete bandgaps of square and hexagonal columns were larger than those of cylindrical columns because of the large number of parameters and, possibly, the localization of the electromagnetic wave at the corner.

Regarding the location of the bandgap in the frequency domain, the complete bandgap for all the three structures lies between the 14th and 15th branches for TE polarization and between the 13th and 14th branches for TM polarization. The band edges for both polarizations occur at different points, with the exception of the square column structure (Table 2). The edge of CPBG generally exists at the corner of the Brillouin zone; however, this condition was not apparent in our triangular array of the hexagonal column structures. As previously mentioned, the hexagonal columns show the maximum CPBG when $x/a = 0.2875$ and $Angle = 43^\circ$ (Figure 1); that is, the angled columns of high- ϵ TiO₂ constitute more than half of the distance between the columns. The Brillouin zone of such a structure might not be considered the same as that of a normal triangular array because we have to additionally consider the smaller hierarchy of hexagonal columns to the larger hierarchy of triangular array. This difference could account for the band edge position.

Table 2. Edge position of the complete photonic bandgap in the triangular arrays of cylindrical, square and hexagonal columns illuminated by transverse-electric (TE) and transverse-magnetic (TM) polarizations.

	Shape	Cylindrical	Square	Hexagonal
TE	Upper edge	K	M	K
	Lower edge	K	M	Between M and K
TM	Upper edge	K and Γ	M	Between Γ and M
	Lower edge	K	M	K

Figure 1. Schematic images and photonic band diagrams of complete-photonic-band 2D structures composed of rutile-TiO₂ columns in electrolytes. Cylindrical (a), square (b) and hexagonal (c) columns were triangularly arrayed and connected by TiO₂ walls. The complete photonic bandgaps are shown as green lines. The maximum gap–midgap ratio appears below the photonic band diagram.

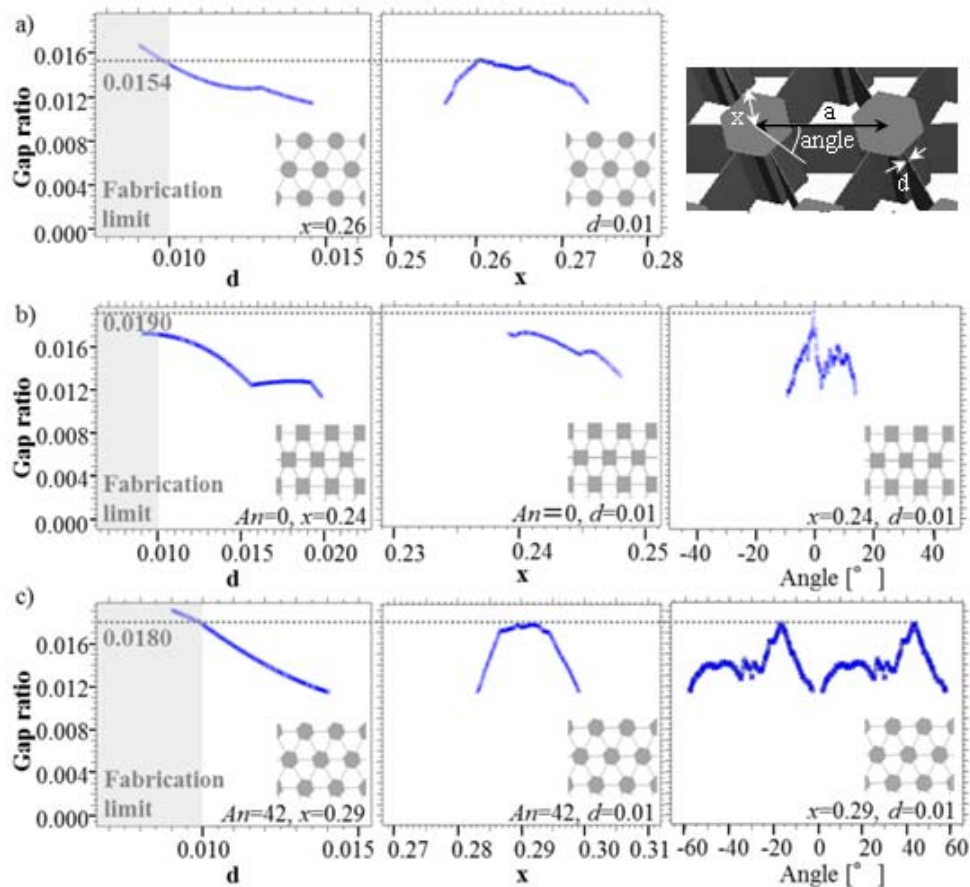


3.2. Gap Ratio Change with Each Parameter

Changes in the gap ratio varied with each parameter are summarized in Figure 2. The $\Delta\omega/\omega_{\text{mid}}$ value increased as d decreased. The strength of the interactions among scattering walls is attributed to the field distribution characteristics. Thus, bandgap can vary significantly depending on the geometric details of photonic crystals [25]. Qiu *et al.* reported that TE polarization bandgap appeared with small wall widths [26]. These results indicate that the wall—that is, the localized spot for TE polarization—plays a key role in obtaining a large complete 2D bandgap in our structures.

The x and $Angle$ were normalized by $d = 0.01$ because $d < 0.01$ (gray area in Figure 2); that is, a thickness of several nanometers for the visible light wavelength is impractical. The $\Delta\omega/\omega_{\text{mid}}$ value did not exhibit a monotonic increase in x because TE polarization shows lower localization at an extremely large x . In hexagonal columns, the $\Delta\omega/\omega_{\text{mid}}$ dependence of $Angle$ —angle is therefore the same as that of $Angle$ 0° to 60° . This result can be easily explained by hexagonal symmetrical geometry. In square columns, a large $\Delta\omega/\omega_{\text{mid}}$ value was observed at a slightly negative angle. The distance between the corner of the square and the wall decreased at the triangular array of slightly negative-angled square columns, resulting in the strong localization of TE polarization.

Figure 2. Maximum gap–midgap ratio dependence on d , x , and $Angle$. Cylindrical (a), square (b), and hexagonal (c) TiO_2 columns were triangularly arrayed and connected by TiO_2 walls. Each fixed parameter is shown in the inset.



4. Conclusions

The photonic bands of various TiO₂ photonic crystals filled with acetonitrile were investigated from the perspective of the dye-sensitized solar cells. Our structural design followed recent discoveries by other researchers: bandgaps for TE polarization are favored in a lattice of an isolated high- ϵ region, bandgaps for TM polarization are favored in a connected lattice, and two geometric parameters are required to balance the band edges of TE and TM polarizations in order to obtain the optimal complete bandgap [20]. The finite-difference time-domain methods on such structures revealed that two-dimensional (2D) photonic crystals with rods connected with walls composed of TiO₂ and electrolyte had complete photonic band gaps under the specific conditions. The maximum gap-midgap ratio dependence on the wall thickness, rod diameter and angle of cylindrical, square, and hexagonal columns was precisely examined. The optimally designed bandgap reaches a large $\Delta\omega/\omega_{\text{mid}}$ value, 1.9%, in a triangular array of square rods connected with walls, which is the largest complete 2D bandgap thus far reported for a photochemical system. These discoveries would promote the photochemical applications of photonic crystals.

Acknowledgments

The authors thank M. Kurihara for her support. This work was partially supported by the Ministry of Education, Culture, Sports, Science and Technology (2170024), Tokuyama Science Foundation, the Kazuchika Okura Memorial Foundation, and Nihon University Strategic Projects for Academic Research (Nanotechnology Excellence).

Conflict of Interest

The authors declare no conflict of interest.

References

1. Tao, C.-A.; Zhu, W.; An, Q.; Li, G. Theoretical demonstration of efficiency enhancement of dye-sensitized solar cells with double-inverse opal as mirrors. *J. Phys. Chem. C* **2010**, *114*, 10641.
2. Matsushita, S.; Suavet, O.; Hashiba, H. Full-photonic-bandgap structures for prospective dye-sensitized solar cells. *Electrochim. Acta* **2010**, *55*, 2398–2403.
3. Guldin, S.; Hüttner, S.; Kolle, M.; Welland, M.E.; Müller-Buschbaum, P.; Friend, R.H.; Steiner, U.; Tétreault, N. Dye-sensitized solar cell based on a three-dimensional photonic crystal. *Nano Lett.* **2010**, *10*, 2303–2309.
4. Kwak, E.S.; Lee, W.; Park, N.-G.; Kim, J.; Lee, H. Compact inverse-opal electrode using non-aggregated TiO₂ nanoparticles for dye-sensitized solar cells. *Adv. Funct. Mater.* **2009**, *19*, 1093–1099.
5. Colodrero, S.; Mihi, A.N.; Häggman, L.; Ocaña, M.; Boschloo, G.; Hagfeldt, A.; Míguez, H.N. Porous one-dimensional photonic crystals improved the power-conversion efficiency of dye-sensitized solar cells. *Adv. Mat.* **2009**, *21*, 764–770.
6. Mihi, A.; Calvo, M.E.; Anta, J.A.; Míguez, H. Spectral response of opal- based dye-sensitized solar cells. *J. Phys. Chem. C* **2008**, *112*, 13–17.

7. Lee, S.-H.A.; Abrams, N.M.; Hoertz, P.G.; Barber, G.D.; Halaoui, L.I.; Mallouk, T.E. Coupling of titania inverse opals to nanocrystalline titania layers in dye-sensitized solar cells. *J. Phys. Chem. B* **2008**, *112*, 14415–14421.
8. Matsushita, S.I.; Fukuda, N.; Shimomura, M. Photochemically functional photonic crystals prepared by using a two-dimensional particle-array template. *Colloid. Surf. A* **2005**, *257–258*, 15–17.
9. Matsushita, S.; Fujiwara, R.; Shimomura, M. Calculation of photonic energy bands of self-assembled-type TiO₂ photonic crystals as dye-sensitized solar battery. *Colloid. Surf. A* **2008**, *313–314*, 617–620.
10. Mihi, A.; Calvo, M.E.; Anta, J.A.; Miguez, H. Spectral response of opal-based dye-sensitized solar cells. *J. Phys. Chem. C* **2008**, *112*, 13–17.
11. Yablonovitch, E. Inhibited spontaneous emission in solid-state physics and electronics. *Phys. Rev. Lett.* **1987**, *58*, 2059–2062.
12. John, S. Strong localization of photons in certain disordered dielectric superlattices. *Phys. Rev. Lett.* **1987**, *58*, 2486–2489.
13. Usami, A. Theoretical study of application of multiple scattering of light to a dye-sensitized nanocrystalline photoelectrochemical cell. *Chem. Phys. Lett.* **1997**, *277*, 105.
14. Nishimura, S.; Abrams, N.; Lewis, B.A.; Halaoui, L.I.; Mallouk, T.E.; Benkstein, K.D.; Lagemaat, J.V.D.; Frank, A.J. Standing wave enhancement of red absorbance and photocurrent in dye-sensitized titanium dioxide photoelectrodes coupled to photonic crystals. *J. Am. Chem. Soc.* **2003**, *125*, 6306–6310.
15. Rehm, J.M.; McLendon, G.L.; Nagasawa, Y.; Yoshihara, K.; Moser, J.; Gratzel, M. Femtosecond electron-transfer dynamics at a sensitizing dye-semiconductor (TiO₂) interface. *J. Phys. Chem.* **1996**, *100*, 9577–9578.
16. Shimomura, M.; Matsushita, S.; Fukuda, N. Photon-to-electron conversion devices and the application to the solar cells. Japanese Unexamined Patent Application Publication No. 2005-72524, 2005.
17. Ritari, T.; Tuominen, J.; Ludvigsen, H.; Petersen, J.C.; Sørensen, T.; Hansen, T.P.; Simonsen, H.R. Gas sensing using air-guiding photonic bandgap fibers. *Opt. Express* **2004**, *12*, 4080–4087.
18. Chen, J.S.Y.; Euser, T.G.; Farrer, N.J.; Sadler, P.J.; Scharrer, M.; Russell, P.S.J. Photochemistry in photonic crystal fiber nanoreactors. *Chem. Eur. J.* **2010**, *16*, 5067–5612.
19. Oh, S.H.; Kim, J.G.; Kim, C.S.; Chang, S.; Lee, S.; Jeong, M.Y. The fabrication of three-dimensional nano-structures by defocused electron beam energy. *Microelectron. Eng.* **2011**, *88*, 914–922.
20. Chern, R.-L.; Chang, C.-C.; Chang, C.C.; Hwang, R.R. Two classes of photonic crystals with simultaneous band gaps. *Jpn. J. Appl. Phys.* **2004**, *43*, 3484–3490.
21. Joannopoulos, J.D.; Johnson, S.G.; Winn, J.N.; Meade, R.D. *Photonic Crystals: Molding the Flow of Light*; Princeton University Press: New Jersey, NJ, USA, 2008.
22. Marsal, L.F.; Trifonov, T.; Rodriguez, A.; Pallares, J.; Alcubilla, R. Larger absolute photonic band gap in two-dimensional air-silicon structures. *Physica E* **2003**, *16*, 580–585.

23. Wang, X.H.; Gu, B.Y.; Li, Z.Y.; Yang, G.Z. Large absolute photonic band gaps created by rotating noncircular rods in two-dimensional lattices. *Phys. Rev. B* **1999**, *60*, 11417.
24. Chern, R.L.; Chang, C.C.; Chang, C.; Hwang, R.R. Large full band gaps for photonic crystals in two dimensions computed by an inverse method with multigrid acceleration. *Phys. Rev. E* **2003**, *68*, 026704.
25. Liu, W.-L.; Yang, T.-J. Engineering the bandgap of a two-dimensional photonic crystal with slender dielectric veins. *Phys. Lett. A* **2007**, *369*, 518–523.
26. Qiu, M.; He, S. Optimal design of a two-dimensional photonic crystal of square lattice with a large complete two-dimensional bandgap. *J. Opt. Soc. Am. B* **2000**, *17*, 1027–1030.

© 2012 by the authors; licensee MDPI, Basel, Switzerland. This article is an open access article distributed under the terms and conditions of the Creative Commons Attribution license (<http://creativecommons.org/licenses/by/3.0/>).